NEW FRONT. CHEM. (**2014**)
Volume 23, Number 1, pp. 61-72
ISSN 2393-2171; ISSN-L 2393-2171

Former: Ann. West Univ. Timisoara – Series Chem.
ISSN: 1224-9513

Article

ADVANCED QSAR AND COMPUTATIONAL MUTAGENESIS APPLIED TO MITOTIC CHECKPOINT PROTEIN HMAD1 MUTANTS WITH IMPLICATION IN GENETIC DISORDERS

Speranta Avram[1,♣], Adina Milac[1,2], Catalin Buiu[3] and Livia-Cristina Borcan[4]

[1] University of Bucharest, Faculty of Biology, Department of Anatomy, Animal Physiology and Biophysics, 91-95th Independentei Str., Bucharest-076201, Romania
[2] Institute of Biochemistry of the Romanian Academy, Structural Biochemistry and Bioinformatics Department, 296th Independentei Str., Bucharest-060031, Romania
[3] Politehnica University of Bucharest, Faculty of Automatic Control and Computers, 113th Independentei Str., Bucharest-040042, Romania
[4] Municipal Clinical Emergency Hospital of Timisoara, Occupational Health Dept., 12th Revolutiei 1989 Bvld., Timisoara-300041, Romania

ABSTRACT

In normal cells, the accuracy of chromosome segregation namely euploidy is ensured by properly functioning error-checking spindle assembly checkpoint. Spindle assembly checkpoint component, human mitotic arrest-deficient protein Mad1 (hMad1) is critical to prevent cellular aneuploidy, and was recognized as an inductor of genetic diseases. Here, we analyzed the capacity of hMad1 mutants in their risk of inducing genetic disorders. Their critical molecular descriptors were calculated and compared by structure–activity relationships in order to elucidate the contribution of these molecular features to initiate genetic disorders. Our results suggest that in the hMad1 mutants descriptors could be deeply involved in aneuploidy.

Keywords: Mad1, cancer, bipolar syndrome, computational mutagenesis.

♣ Correspondent author: Tel: 0040740234158, Fax: 0040213181573, E-mails: speranta.avram@gmail.com

1. INTRODUCTION

During mitotic cell division, exact copies of cell chromosomes are obtained and pairs of sister chromatids are produced [1,2]. Furthermore, these are attached to microtubules originating from two opposite spindle poles by kinetochores (protein structure on chromatids) during a bi-orientation process [1,3,4]. A judicious bi-orientation mechanism leads to euploidy, but, sometimes, the premature separation of a single pair of sister chromatids may lead to aneuploidy [4]. Therefore, the cells develop a control system called the mitotic spindle assemble checkpoint (SAC), which delays the onset of anaphase until all sister chromatid pairs have performed the bi-orientation process [5-7].

The SAC complex is formed by many proteins including Bub1, BubR1, Bub3, Mps1, Mad1 and Mad2, which are recruited to unattached kinetochores to prevent aneuploidy [5]. The functional mechanism of SAC involves interactions among these proteins; Mad1-Mad2 core complex represents the key catalytic engine of the SAC [8]. It is important to mention that the Mad1-Mad2 core complex catalyses the conformational activation of the unusual two-state protein Mad2 [9-16].

Biochemically, the hMad1 amino acid sequence is 718 residues long and is highly conserved from yeast to human. Crystallographic studies [5,17,18] revealed that: (i) hMad1 is an elongated protein, which works as a dimer; (ii) residues 485-584 are critical for Mad1-Mad2 binding and stabilisation of the Mad1 dimer, therefore; (iii) mutations in this region destabilise the Mad1–Mad2 complex and the Mad1-Mad1 dimer. Structure-based mutagenesis and clinical studies [18-21] showed that mutations in the Mad1-Mad2 binding motif, 500-580 amino acids, critically affect SAC activity, and represent a major form of genomic instability in human cancers [19-21] or bipolar disorder (BD) [22]. A recent study by Cichon *et al.* [22] demonstrated a significant genome-wide association between hMad1 on 7p22.3 and an excess of T alleles in patients with BD. The same genetic variation of hMad1 on 7p22.3 was also found in patients with cancer [20,22], where the following hMad1 mutants were identified: R59C, T500M and R556C. Nomoto *et al.* [19] and Tsukasaki *et al.* [20] identified hMad1 mutations R59C, T299A, T500M, E511K, E516K, R556C, E569K and R572H as being involved in the pathogenesis of a variety of human cancers, including lymphomas, lung, prostate and breast cancers, and glioblastomas.

Despite numerous *in vivo* and *in vitro* studies connecting aneuploidy with hMad1 mutations, its complex structural and functional profile hindered a complete understanding of aneuploidy mechanisms. Encouraged by the large amount of clinical and experimental data, and also considering the reduced number of computational and crystallographic studies, we aimed to use structure–activity relationship (SAR) analysis to rationalise the capacity of established hMad1 mutants to induce aneuploidy and design new aneuploidy-inducing mutants by computational mutagenesis.

All SAR methods consider that macroscopic properties are induced by molecular structure, and every change in molecular structure leads to modification of these properties [23]. Considering that hMad1 is widely involved in many types of genetic diseases, the design and analysis of new hMad1 mutants appears to be a necessity in preclinical and clinical studies. However, prediction accuracy of protein function is dependent on the appropriate selection of physical and chemical properties of proteins. Usually, the selection of

effective molecular descriptors is problem-dependent and there is no universal rule to achieve this goal.

We previously developed SAR models [24,25] for viral proteins and antimicrobial activity of peptides, and proposed new, more effective analogues, which suggest that molecular descriptors, including hydrophobic features, steric (e.g., molecular surface area) or count of atom types, are critical for biological activity.

In the present study, we attempt to generate highly accurate SAR models of cellular proteins by using computational methods, and to explore new perspectives for understanding the mechanism of aneuploidy and its implication in genetic diseases. Thus, we establish variations in molecular descriptors, such as electronic fields and protein surface areas, which described hMad1 wild type (wt) and other mutant forms, and we calculate the values of these descriptors in cases of aneuploidy.

2. METHODS

2.1. Dataset for analysis: molecular modeling minimum energy calculation strategy of classical and *de novo* hMAD1 mutants

Based on experimental data demonstrating that hMad1 residues 493-584 are critical for Mad1-Mad2 interactions, we generated hMad1 mutants from a hMad1 wt template available from crystallographic structures (PDB: 1GO4) [5,18]. The database of hMad1 mutants was generated according to the following criteria: (i) the range of observed destabilisation of hMad1 function, and also the variability of cellular lines expressing these mutants [5,19,20]; and (ii) the variety of amino acids that were replaced in the hMad1 structure. In agreement with experimental data [20,21], we chose to analyse aneuploidy induced by eight hMad1 mutants that are deeply involved in promoting many types of cancers, and probably BD: T500M (numerous cancer types and possibly BD), E511K (lung cancer), E516K (numerous cancer types), R556C (prostate cancer and probably BD), R556H (lung cancer), R558H (numerous cancer types), E569K (breast cancer), and R572H (numerous cancer types). Furthermore, in our study, we included hMad1 C568D, L571D, L575D, P549A, M545A, and L543A mutants, which completely abolished or significantly reduced Mad1-Mad2 binding [18].

An important objective of the study was to determine the molecular features of *de novo* hMad1 mutants susceptible to induce aneuploidy. *De novo* hMad1 mutants were designed following several general rules: (i) the electrostatic contacts were changed by introducing positively charged amino acids: for example, R, K and H; (ii) the number of hydrophobic contacts was varied by introducing very hydrophobic amino acids F, I and W; (iii) we changed the hydrogen bond donor/acceptor character by introducing R and K; and (iv) the molecular surface areas were changed by substitutions with small amino acids, such as A or G, or the bulky amino acid W. The mutations were: T500/S/N/L/W; E511/R/D/N/Q; E516/T/M/F/L; R556/K/L/F/I; R558/A/W/M/G; E569/D/Q/P/W; and R572/K/L/F/I, and we aimed to analyses whether the replacements of these amino acids were able, or not, to induce

aneuploidy by changing the values of molecular descriptors in comparison with hMad1 mutants template.

Molecular modeling of all dimer hMad1 mutants was performed using Insight software package (Accelrys, Inc., San Diego, CA, USA) and the minimum potential energy was calculated using conjugate gradient method, Kollman force-field [26]. After energy minimisation, Kollman partial charges [27] of the compounds were loaded. During energy minimisation, free movement of only the amino acid side chains was allowed.

2.2. Descriptors Calculation

Molecular descriptors of hMad1 wt and mutants were calculated using a database from MOE software (Chemical Computing Group, Montreal, PQ, Canada). The following considerations were critical for our study: solvation energy [28-30], and surface areas represented by: (i) subdivided van der Waals surface induced by hydrophobic and polar atoms (vsa_hyd, vsa_pol) [31,32]; (ii) subdivided solvent accessible surface areas induced by hydrophobic and polar atoms (ASA_hyd, ASA_pol) [31,32]; and (iii) subdivided solvent accessible surface areas induced by atoms with positive and, respectively, negative partial charges (ASA_pos, ASA_neg) [31,32].

3. RESULTS AND DISCUSSIONS

3.1. Results

The initial stage of our study results was represented by the evaluation of molecular descriptors described as hMad1 mutants already recognised as aneuploidy risk factors. Table 1 illustrates the molecular descriptors, showing significant fluctuations among hMad1 wt and mutant forms in the domain of residues 493-579.

Table 1: Molecular descriptors of Mad1 wt, Mad1 mutants recognized as aneupoidy inductors and *de novo* Mad 1 mutants obtained by computational mutagenesis

	Mad1 mutants	**E_sol (kcal/mol)**	**ASA_hyd ($Å^2$)**	**ASA_pol ($Å^2$)**	**vsa_pol ($Å^2$)**	**vsa_hyd ($Å^2$)**
Literature-based Mad1 mutants	Mad1 wt	-3440.56	8038.16	8096.00	6407.53	9148.24
	T500M	-3425.01	8117.24	8127.62	6380.40	9241.98
	E511K	-3381.12	8016.23	8149.42	6388.75	9220.46
	E516K	-3772.79	8078.25	8127.11	6388.75	9220.46
	R556C	-3451.54	8130.51	7887.33	6306.41	9152.19
	R556H	-3447.66	8202.24	7874.16	6329.14	9202.24
	R558H	-3332.45	8113.44	8036.75	6347.93	9130.02
	E569K	-3339.45	8230.46	8028.22	6388.75	9220.46
	R572H	-3297.43	8117.45	7946.56	6347.93	9130.02

	C568D	-3666.90	7985.85	8154.24	6461.80	9144.29
	L571D	-3711.79	7984.28	8191.37	6461.80	9026.19
	L575D	-3638.83	7930.12	8201.30	6461.80	9026.19
	P549A	-3421.79	7981.65	8106.42	6418.90	9103.22
	M545A	-3440.23	7949.46	8028.85	6407.53	9037.58
	L543A	-3442.74	7984.72	8112.76	6407.53	9053.39
Mad1 mutants obtained by computational mutagenesis	T500S	-3445.56	8001.18	8131.80	6407.53	9116.62
	T500N	-3451.80	7936.60	8211.96	6443.02	9104.12
	T500L	-3422.44	8137.09	8051.45	6380.40	9226.17
	T500W	-3432.09	8179.84	8088.32	6391.76	9293.42
	E511R	-3463.14	8008.27	8137.66	6435.60	9188.84
	E511D	-3500.77	8010.21	8126.05	6407.53	9116.62
	E511N	-3333.94	8004.45	8129.04	6415.88	9116.62
	E511Q	-3332.58	8039.37	8112.29	6415.88	9148.24
	E516T	-3468.94	8078.86	8063.83	6380.40	9160.74
	E516M	-3436.26	8082.69	8047.83	6353.26	9254.48
	E516F	-3448.75	8160.88	7970.12	6353.26	9279.12
	E516L	-3457.11	8122.52	8012.13	6353.26	9238.67
	R556K	-3436.89	8140.18	7966.52	6360.68	9179.86
	R556L	-3419.87	8210.59	7823.62	6325.20	9198.07
	R556F	-3433.85	8291.84	7796.59	6325.20	9238.53
	R556I	-3421.07	8171.81	7827.23	6325.20	9198.07
	R558A	-3303.95	8093.54	7983.20	6325.20	9103.22
	R558W	-3311.90	8283.18	7957.10	6336.56	9265.32
	R558M	-3305.30	8164.38	8033.89	6325.20	9213.88
	R558G	-3303.43	8054.63	8003.68	6325.20	9071.61
	E569D	-3530.94	7983.52	8110.04	6407.53	9116.62
	E569Q	-3436.41	8013.90	8171.54	6415.88	9148.24
	E569P	-3422.37	8059.33	8009.68	6341.90	9188.84
	E569W	-3427.01	8193.79	7976.28	6364.63	9305.92
	R572K	-3481.57	8091.42	8051.23	6360.68	9179.86
	R572L	-3396.79	8151.87	7908.00	6325.20	9198.07
	R572F	-3400.69	8222.90	7871.26	6325.20	9238.53
	R572I	-3395.02	8140.85	7903.32	6325.20	9198.07

Different variations of molecular descriptors, such as subdivided van der Waals surface areas, were recorded in hMad1 wt and mutants in the domain of residues 493-579. To better emphasize the variation of different parameters for various mutants, and due to the fact that the absolute numeric values of descriptors are high, we plotted the difference between subdivided molecular surface area values calculated for hMad1 mutants and wt in Figure 1 and 2. Figure 1 demonstrates that the presence of hydrophobic residues induces a significant fluctuation of van der Waals surface areas (vsa_hyd) compared with a weak fluctuation of the van der Waals surface areas induced by polar (vsa_pol) amino acid residues. In addition,

Figure 2 shows that the presence of hydrophobic, polar and charged atoms induces fluctuation of solvent accessible surface area.

Figure 1: Dot-plot representation of the van der Waals area components given by hydrophobic and polar atoms (values are calculated as the difference between various mutants and wild type Mad1; black diamonds correspond to mutations: T500M, E511K, E516K, R556C, R556H, R558H, E569K, and R572H; grey diamonds correspond mutations: C568D, L571D, L575D, P549A, M545A, and L543A; open diamonds correspond to computationally induced mutations)

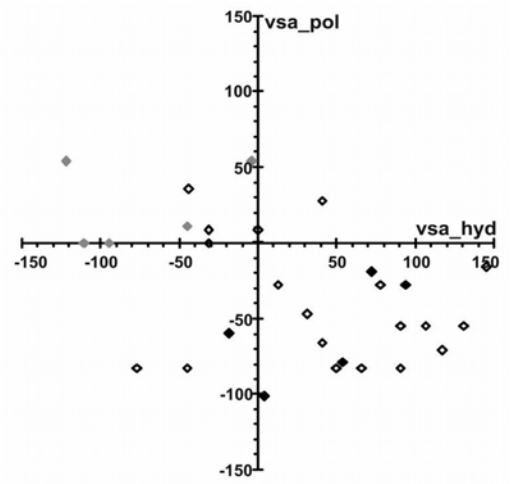

Figure 2: Dot-plot representation of the solvent accessible surface area components corresponding to the polar and hydrophobic atoms (values are calculated as the difference between various mutants and wild type Mad1; black diamonds correspond to mutations: T500M, E511K, E516K, R556C, R556H, R558H, E569K, and R572H; grey diamonds correspond to mutations: C568D, L571D, L575D, P549A, M545A, and L543A; open diamonds correspond to computationally induced mutations)

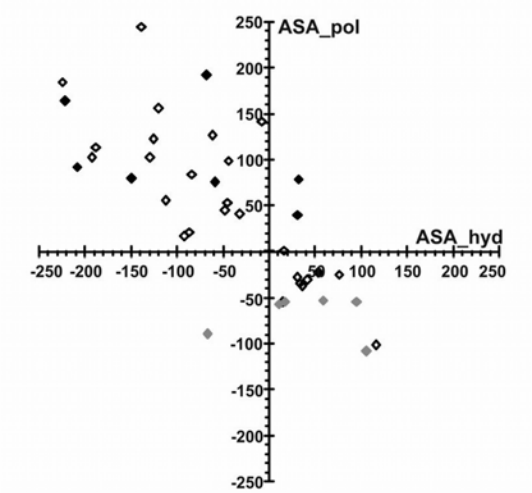

3.2. Discussion

Based on the SAR hypothesis, stating that molecular descriptors of proteins are able to suggest their function, we performed a study comparing molecular descriptors, identified as critical, in native and mutants hMad1 in the domain of residues 493-579, which is strongly involved in Mad1-Mad2 binding and already recognized as a cellular euploidy factor. Furthermore, to provide a new interpretation of aneuploidy mechanism, based on molecular descriptors evaluation, we induced, by computational mutagenesis, a number of hMad1 mutants and analyzed these mutants as possible aneuploidy inductors.

In our study, we classified and analyzed the molecular descriptors in a few clusters: (i) the potential energy cluster including solvation, van der Waals, electrostatic and torsion energies; (ii) the molecular surface cluster containing subdivided van der Waals and solvent accessible surface areas; and (iii) the structural cluster comprising molecular descriptors derived directly from protein sequence atoms (polar/hydrophobic/hydrogen bond donor–acceptor) and bond type (rigid and rotatable) counts.

Molecular descriptors of hMad1 mutants in the domain of residues 493-579, especially potential energy descriptors, undergo significant variation with solvation energy changing from -3772.79 kcal/mol (E516K) to -3297.43 kcal/mol (R572H), and torsion energy changing from 952.15 kcal/mol (T500L) to 972.96 kcal/mol (R558M).

Cluster analysis of solvation energy indicates that hMad1 wt and the hMad1 mutant M545A have almost identical values (-3440.56 kcal/mol vs. -3440.23 kcal/mol). Other very similar values of solvation energy were obtained for four *de novo* mutants: L543A (-3442.74 kcal/mol), R556K (-3436.89 kcal/mol), E569Q (-3436.41 kcal/mol) and E516M (-3436.26 kcal/mol; Table 1). We may presume that, in this respect, these hMad1 mutants, induced by computational mutagenesis, have a small risk to induce cellular aneuploidy.

A similar interpretation may be given to the substitution of smaller-sized positively charged amino acid R572 with non-polar amino acids L, F and I, and the bulky positive amino acid K. A comparison between the values of solvation energy of hMad1 wt and these hMad1 mutants (see Table 1), suggests that these mutants have a low chance of inducing various types of cancer. This observation is supported by: (i) experimental data [19,20] showing that hMad1 R572H induces many types of cancer; and (ii) findings that the solvation energy values for mutants R572/L/F/I/K are closer to hMad1 wt than to the pathological hMad1 R572H mutant (Table 1). On the other hand, the solvation energy value of hMad1 wt is significantly different from that of the naturally occurring hMad1 R572H mutant (-3297.43 kcal/mol) and those of *de novo* mutants: R558G (-3303.43 kcal/mol), R558M (-3305.30 kcal/mol) and R558A (-3303.95 kcal/mol). Based on the experimental data mentioned above and on our computational results, it can be stated that, energetically, the above-mentioned *de novo* hMad1 mutants may induce the same cancer types as the R572H mutant.

In Figure 3, we represent the solvation energy variation of mutants at several positions (indicated on the bottom line) towards the value for the wt hMad1. The position of these residues on the protein structure is illustrated in the top panel.

Figure 3: Variation of the solvation energy between various Mad1 mutants and the wild type protein (different mutations at the same position in the wild type protein (shown on the bottom line) are indicated by the same background shade; the specific target mutation is indicated by letters near each column; the top image indicates the position of each mutated residue in the Mad1 structure (PDB: 1GO4); for simplicity, only those mutants whose descriptors demonstrated variations above 4% are shown)

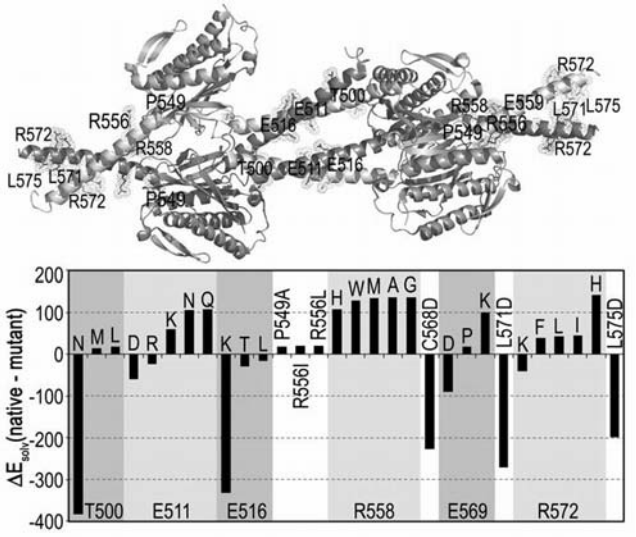

For hMad1 mutants, the analysis of subdivided van der Waals descriptors cluster (Figure 4) indicates that: (i) a vsa_hyd varies significantly in the range between 9026.19 $Å^2$ (L575D) and 9305.92 $Å^2$ (E569W); and (ii) a relatively small variation was found for vsa_pol (from 6306.41 $Å^2$ (R556C) to 6461.80 $Å^2$ (C568D)).

In Figure 4, we presented the difference between values of vsa_hyd area for the hMad1 wt and its various mutants. Mutations inducing large variations of descriptor values have a higher probability of inducing pathologies such as cancer or BD.

Figure 4: Variation of the hydrophobic component of the van der Waals surface area between various Mad1 mutants and the wild type protein (different mutations at the same position in the wild type protein (shown on the bottom line) are indicated by the same background shade)

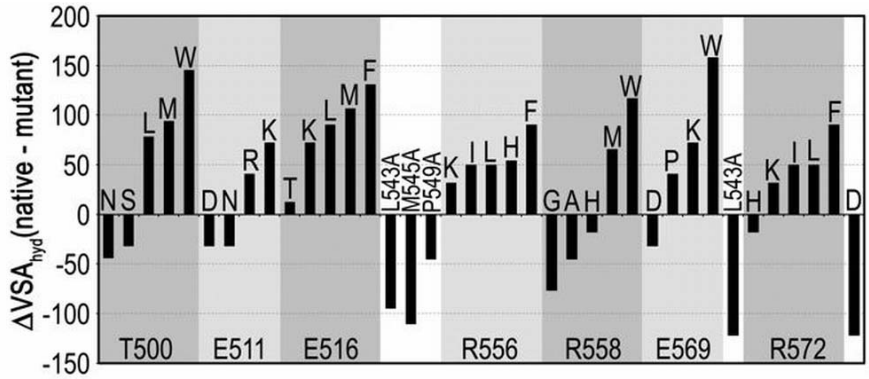

The specific target mutation is indicated by letters near each column. For simplicity, only those mutants whose descriptors demonstrated variations above 4% are shown.

In our study, the value of vsa_hyd area for hMad1 wt was 9148.24 $Å^2$ and the value of vsa_pol area for hMad1 wt was 6407.13 $Å^2$. Our results suggest that, sterically, *de novo* hMad1 mutants E511Q (9148.24 $Å^2$) and E569Q (9148.24 $Å^2$) are less likely to induce aneuploidy. Within the same series of Mad1 mutants, when arginine, threonine and glutamic acid were replaced with bulky hydrophobic tryptophan, phenylalanine or methionine, vsa_hyd values varied within the range of 9250-9300 $Å^2$: E516M (9254.48 $Å^2$), R558W (9265.32 $Å^2$), E516F (9279.12 $Å^2$), T500W (9293.42 $Å^2$), and E569W (9305.92 $Å^2$). We suggest that these *de novo* mutants may induce various types of cancer or BD, given the similarity between their vsa_hyd area values with those of the hMad1 T500M mutant (9241.98 $Å^2$) and the clinical data proving that the hMad1 T500M mutant induces various types of cancer or BD (20, 21, 24, 25).

Analysis of the subdivided solvent accessible surface area variations showed the following fluctuations: ASA_pol maximum and minimum values of 8211.96 $Å^2$ (T500N) and 7796.59 $Å^2$ (R556F), respectively, and ASA_hyd maximum and minimum values of 8291.84 $Å^2$ (R556F) and 7930.12 $Å^2$, respectively. Cluster analysis of solvent accessible surface areas demonstrated very similar ASA_pol values between hMad1 wt (8096.00 $Å^2$) and the *de novo* mutant T500W (8088.32 $Å^2$), suggesting that this mutation is sterically less likely to induce aneuploidy. On the contrary, other *de novo* mutants, such as R556L (7823.62 $Å^2$) and R556I (7827.23 $Å^2$), have very similar ASA_pol values with R556H (7874.16 $Å^2$) and R556C (7887.33 $Å^2$). In conjunction with experimental data showing that hMad1 R556C and R556H induced prostate and lung cancer, and probably psychiatric disorders [19,20], our computational data support the hypothesis that hMad1 R556L and R556I mutants induce the same pathologies.

When subdivided solvent accessible surface area are considered as an aneuploidy factor, we presume that various *de novo* hMad1 mutants may fail to induce different types of cancer when they have the following molecular features: (i) ASA_hyd around values of hMad1 wt (8038.16 $Å^2$, e.g., E511Q (8039.37 $Å^2$)); (ii) ASA_pol around values of hMad1 wt (8096.00 $Å^2$, e.g., T500W (8088.32 $Å^2$)); or (iii) solvent accessible surface areas induced by atoms with a positive partial charge around values of hMad1 wt (11367.97 $Å^2$, e.g., R556K (11365.23 $Å^2$); Table 1 and Figure 1, 2 and 4).

We have to mention that the lack of experimental data regarding *de novo* hMad1 mutants imposes significant limitations on the impact of our study. Even though the biological processes in which hMad1 are involved are very complex and difficult to replicate *in vivo*, the extension of our study by *in vivo* analyses of these *de novo* mutants is crucial.

4. CONCLUSIONS

Molecular simulation techniques such as rational design of protein mutants and structural – enzymatic activity relations will continue to reveal important information about protein function or implication of proteins in many cellular processes such as correct chromosome segregation (euploidy), but it is important to understand the limitations and problems of these

techniques. In our study a number of Mad1 mutants (already known to induce aneuploidy and proposed by us by computational mutagenesis), at distinct domain: 493-579 (strongly involved into Mad1-Mad2 binding already recognized to affect cellular euploidy) were considered.

These mutants were analyzed relatively to structural descriptors in correlation with destabilization of SAC activity and also inducing genetic diseases like cancer and BD. Among various structural descriptors considered in our study, the steric (van der Waals area and solvent accessible area and their subdivided) and also energetic solvation energy descriptor are more relevant for our ability to predict genetic pathologies and their mechanism of action, for the development of effective methods for early diagnosis and for possible treatment strategies. We concluded that the evaluation of solvation energy of the Mad1 amino acids and also, in equal manner the van der Waals and the solvent accessible surface areas over all hydrophobic/polar and positively charged atoms may be important for predicting by molecular simulation techniques the aneuploidy inductor role of Mad1 mutants. We suggested that the Mad1 wild-type and mutants molecular descriptors evaluated here represent important resources for future computational studies focused on aneuploidy, provided kinetic data about Mad1-Mad2 and/or Mad1-Bub3 are available.

ACKNOWLEDGEMENT

Funding: Speranta Avram acknowledges support from the Romanian National Authority for Scientific Research grant CNMP PNII 89/2012, grant PNII-PCCA-16/2012 and PC7 ERA-NET HIVERA.

REFERENCES

1. Yu, H. Structural activation of Mad2 in the mitotic spindle checkpoint: the two-state Mad2 model versus the Mad2 template model. *J Cell Biol* **2006**, *173*, 153–157.
2. Koshland, D.E.; Guacci, V. Sister chromatid cohesion: the beginning of a long and beautiful relationship. *Curr Opin Cell Biol* **2000**, *12*, 297–301.
3. Cleveland, D.W.; Mao, Y.; Sullivan, K.F. Centromeres and kinetochores: from epigenetics to mitotic checkpoint signaling. *Cell* **2003**, *112*, 407–421.
4. Tanaka, K.; Mukae, N.; Dewar, H.; van Breugel, M.; James, E.K.; Prescott, A.R.; Antony, C.; Tanaka, T.U. Molecular mechanisms of kinetochore capture by spindle microtubules. *Nature* **2005**, *434*, 987–994.
5. Kim, S.; Sun, H.; Tomchick, D.R.; Yu, H.; Luo, X. Structure of human Mad1 C-terminal domain reveals its involvement in kinetochore targeting. *Proc Natl Acad Sci USA* **2012**, *109*, 6549–6554.
6. Musacchio, A.; Salmon, E.D. The spindle-assembly checkpoint in space and time. *Nat Rev Mol Cell Biol* **2007**, *8*, 379–393.
7. Musacchio, A.; Ciliberto, A. The spindle-assembly checkpoint and the beauty of self-destruction. *Nat Struct Mol Biol* **2012**, *19*, 1059–1061.
8. Schuyler, S.C.; Wu, Y.F.; Kuan, V.J. The Mad1-Mad2 balancing act – a damaged spindle checkpoint in chromosome instability and cancer. *J Cell Sci* **2012**, *125*, 4197–4206.

9. Luo, X.; Tang, Z.; Xia, G.; Wassmann, K.; Matsumoto, T.; Rizo, J.; Yu, H. The Mad2 spindle checkpoint protein has two distinct natively folded states. *Nat Struct Mol Biol* **2004**, *4*, 338–345.
10. Mapelli, M.; Massimiliano, L.; Santaguida, S.; Musacchio, A. The Mad2 conformational dimer: structure and implications for the spindle assembly checkpoint. *Cell* **2007**, *4*, 730–743.
11. Mapelli, M.; Filipp, F.V.; Rancati, G.; Massimiliano, L.; Nezi, L.; Stier, G.; Hagan, R.S.; Confalonieri, S.; Piatti, S.; Sattler, M.; Musacchio, A. Determinants of conformational dimerization of Mad2 and its inhibition by p31com. *EMBO J* **2006**, *6*, 1273–1284.
12. Izawa, D.; Pines, J. Mad2 and the APC/C compete for the same site on Cdc20 to ensure proper chromosome segregation. *J Cell Biol* **2012**, *1*, 27–37.
13. Kulukian, A.; Han, J.S.; Cleveland, D.W. Unattached kinetochores catalyze production of an anaphase inhibitor that requires a Mad2 template to prime Cdc20 for BubR1 binding. *Dev Cell* **2009**, *1*, 105–117.
14. Tischer, T.; Hörmanseder, E.; Mayer, T.U. The APC/C inhibitor XErp1/Emi2 is essential for *Xenopus* early embryonic divisions. *Science* **2012**, *6106*, 520–524.
15. Jia, L.; Li, B.; Warrington, R.T.; Hao, X.; Wang, S.; Yu, H. Defining pathways of spindle checkpoint silencing: functional redundancy between Cdc20 ubiquitination and p31(comet). *Mol Biol Cell* **2011**, *22*, 4227–4235.
16. Kim, S.; Yu, H. Mutual regulation between the spindle checkpoint and APC/C. *Semin Cell Dev Biol* **2011**, *6*, 551–558.
17. De Antoni, A.; Pearson, C.G.; Cimini, D.; Canman, J.C.; Sala, V.; Nezi, L.; Mapelli, M.; Sironi, L.; Faretta, M.; Salmon, E.D.; Musacchio, A. The Mad1/Mad2 complex as a template for Mad2 activation in the spindle assembly checkpoint. *Curr Biol* **2005**, *3*, 214–225.
18. Sironi, L., Mapelli, M., Knapp, S., De Antoni, A., Jeang, K.T., Musacchio, A. Crystal structure of the tetrameric Mad1–Mad2 core complex: implications of a 'safety belt' binding mechanism for the spindle checkpoint. *EMBO J* **2002**, *10*, 2496–2506.
19. Nomoto, S.; Haruki, N.; Takahashi, T.; Masuda, A.; Koshikawa, T.; Takahashi, T.; Fujii, Y.; Osada, H.; Takahashi, T. Search for *in vivo* somatic mutations in the mitotic checkpoint gene, *hMAD1*, in human lung cancers. *Oncogene* **1999**, *50*, 7180–7183.
20. Tsukasaki, K.; Miller, C.W.; Greenspun, E.; Eshaghian, S.; Kawabata, H.; Fujimoto, T.; Tomonaga, M.; Sawyers, C.; Said, J.W.; Koeffler, H.P. Mutations in the mitotic check point gene, *MAD1L1*, in human cancers. *Oncogene* **2001**, *25*, 3301–3305.
21. Cahill, D.P., da Costa, L.T.; Carson-Walter, E.B.; Kinzler, K.W.; Vogelstein, B.; Lengauer, C. Characterization of *MAD2B* and other mitotic spindle checkpoint genes. *Genomics* **1999**, *2*, 181–187.
22. Cichon, S.; Mühleisen, T.W.; Degenhardt, F.A.; Mattheisen, M.; Miró, X.; Strohmaier, J.; Steffens, M.; Meesters, C.; Herms, S.; Weingarten, M.; Priebe, L.; Haenisch, B.; Alexander, M.; Vollmer, J.; Breuer, R.; Schmäl, C.; Tessmann, P.; Moebus, S.; Wichmann, H.E.; Schreiber, S.; Müller-Myhsok, B.; Lucae, S.; Jamain, S.; Leboyer, M.; Bellivier, F.; Etain, B.; Henry, C.; Kahn, J.P.; Heath, S.; Bipolar Disorder Genome Study (BiGS) Consortium; Hamshere, M.; O'Donovan, M.C.; Owen, M.J.; Craddock, N.; Schwarz, M.; Vedder, H.; Kammerer-Ciernioch, J.; Reif, A.; Sasse, J.; Bauer, M.; Hautzinger, M.; Wright, A.; Mitchell, P.B.; Schofield, P.R.; Montgomery, G.W.; Medland, S.E.; Gordon, S.D.; Martin, N.G.; Gustafsson, O.; Andreassen, O.; Djurovic, S.; Sigurdsson, E.; Steinberg, S.; Stefansson, H.;

Stefansson, K.; Kapur-Pojskic, L.; Oruc, L.; Rivas, F.; Mayoral, F.; Chuchalin, A.; Babadjanova, G.; Tiganov, A.S.; Pantelejeva, G.; Abramova, L.I.; Grigoroiu-Serbanescu, M.; Diaconu, C.C.; Czerski, P.M.; Hauser, J.; Zimmer, A.; Lathrop, M.; Schulze, T.G.; Wienker, T.F.; Schumacher, J.; Maier, W.; Propping, P.; Rietschel, M.; Nöthen, M.M. Genome-wide association study identifies genetic variation in neurocan as a susceptibility factor for bipolar disorder, *Am. J. Hum. Genet.* **2011**, *3*, 372–381.

23. Akamatsu, M. Current state and perspectives of 3D-QSAR. *Curr Top Med Chem* **2002**, *12*, 1381–1394.
24. Avram, S.; Duda-Seiman, D.; Borcan, F.; Radu, B.; Duda-Seiman, C.; Mihailescu, D. Evaluation of antimicrobial activity of new mastoparan derivatives using QSAR and computational mutagenesis. *Int J Pept Res Ther* **2011**, *17*, 7–17.
25. Avram, S.; Mihailescu, D.F.; Borcan, F.; Milac, A.L. Prediction of improved antimicrobial mastoparan derivatives by 3D-QSARCoMSIA/CoMFA and computational mutagenesis. *Monatsh Chem* **2012**, *143*, 535–543.
26. Gellért, A.; Salánki, K.; Náray-Szabó, G.; Balázs, E. Homology modelling and protein structure based functional analysis of five cucumovirus coat proteins. *J Mol Graph Model* **2006**, *5*, 319–327.
27. Henriques, J.; Costa, P.J.; Calhorda, M.J.; Machuqueiro, M. Charge parametrization of the DvH-c3 heme group: validation using constant-(pH,E) molecular dynamics simulations. *J Phys Chem B* **2013**, *1*, 70–82.
28. Talavera, D.; Robertson, D.L.; Lovell, S.C. Characterization of protein–protein interaction interfaces from a single species, *PLoS One* **2011**, *6*, e21053.
29. Eisenberg, D.; McLachlan, A.D. Solvation energy in protein folding and binding. *Nature* **1986**, *319*, 199–203.
30. Pei, J.; Wang, Q.; Zhou, J.; Lai, L. Estimating protein–ligand binding free energy: atomic solvation parameters for partition coefficient and solvation free energy calculation. *Proteins* **2004**, *4*, 651–664.
31. Li, A.J.; Nussinov, R. A set of van der Waals and coulombic radii of protein atoms for molecular and solvent-accessible surface calculation, packing evaluation, and docking. *Proteins* **1998**, *1*, 111–127.
32. Bhat, S.; Purisima, E.O. Molecular surface generation using a variable-radius solvent probe. *Proteins* **2006**, *1*, 244–261.